Facile one step green synthesis of iron nanoparticles using grape leaves extract: textile dye decolorization and wastewater treatment

Chandra Devi Raman, Kanmani Sellappa and Martin Mkandawire

ABSTRACT

The existing knowledge on the reactivity of green iron particles on textile dye and wastewater decolorization is very limited. In this study, the potential of green iron particles synthesized using grape leaves extract on reactive dye (reactive red 195, reactive yellow 145, reactive blue 4 and reactive black 5) decolorization were investigated. 95–98% of decolorization was achieved for all reactive dyes at 1.4–2.0 g/L of green iron. Maximum decolorization was attained at lower dye concentration and showed very little impact on decolorization when pH was increased from 3 to 11. The pseudo-first-order fit confirms the reaction between iron particles and dye molecules with rate constant 0.317–0.422 and it is followed by adsorption, data fit with pseudo-second-order model. Hence, not only adsorption but also the reduction process is involved in the reactive dye decolorization. Benzene, phenyl sodium, 2-chloro-1,3,5-triazine, naphthalene, sodium benzene sulfonate, benzene 1,2 di amine, anthracene-9,10 dione, aniline, phenol, benzene sulfonic acid were the major intermediates detected in dye decolorization and the respective reaction pathway is proposed. Green iron from grape leaves extract demonstrated better performance and it is recognized as the promising cost-effective material for textile wastewater treatment.

Key words | dye decolorization pathway, grape leaves extract, green iron particles, textile wastewater treatment

Chandra Devi Raman (corresponding author)
Martin Mkandawire
Department of Chemistry, School of Science and Technology,
Cape Breton University,
Sydney, Nova Scotia,
Canada
E-mail: *chandra_raman@cbu.ca*

Chandra Devi Raman
Department of Civil Engineering,
Anna University,
Chennai, Tamil Nadu,
India

Kanmani Sellappa
Centre for Environmental Studies,
Anna University,
Chennai, Tamil Nadu,
India

HIGHLIGHTS

- Green iron particles synthesized from grape leaves extract.
- Reactivity of bare and green iron particles on textile dye decolorization.
- Dye decolorization pathway proposed.
- Efficiency of green iron particles on textile wastewater decolorization.
- Economic feasibility of synthesized green iron particles on textile wastewater treatment.

INTRODUCTION

The world is facing a global water quality crisis. Population growth, urbanization and industrialization have accelerated the consumption of freshwater and thereby increased the unregulated or illegal discharge of contaminated water to the environment (Corcoran *et al.* 2010). An estimated 80% of all industrial and municipal wastewater are released to the environment without any prior treatment, resulting in a growing deterioration of overall quality with harmful impacts on human health and ecosystems (UNESCO 2018). One such industry is textile dyeing, which consumes enormous amount of water, dyes, chemicals and generates huge amount of colored wastewater (Ghaly *et al.* 2014; Pattnaik *et al.* 2018; Hynes *et al.* 2020). Most of the textile

doi: 10.2166/wst.2021.140

dyes utilized during the dyeing process get washed away in the wastewater and the conventional treatment methods failed to remove the dye color (Holkar *et al.* 2016; Paździor *et al.* 2019). Textile dyes are toxic, recalcitrant in the environment and therefore the degradation of textile dyes is more challenging (Ventura-camargo & Marin-morales 2013).

The application of nanotechnology in environmental remediation has been examined in the last decade and the potential of iron nanoparticles in removing various contaminants like chlorinated, halogenated aliphatic, nitrates, nitro aromatic carbons, heavy metals, phenols, inorganic species, explosives and pesticides has been successfully reported (Fu *et al.* 2014). Textile dye decolorization using nano size iron particles is emerging in the recent years as the particles are highly reactive, non-toxic, and cost-effective (Patil *et al.* 2016). Iron particles aggregate quickly with respect to time and addition of supports could enhance the stability. However, the dye decolorization in the presence of supports such as biochar, clay (kaolin, bentonite, montmorillonite), zeolite (rectorite, clinoptilolite, perlite), resins, heavy metals are observed as an environmental risk, as the supports transfer the adsorbed textile dye to various environments (Raman & Kanmani 2016; Hynes *et al.* 2020). In recent years, plant based green supports are introduced and acclaimed for cost-effective and eco-friendly treatment (Machado *et al.* 2013; Raman & Kanmani 2016; Ozkan *et al.* 2018; Lohrasbi *et al.* 2019; Bhuiyan *et al.* 2020; Ting & Chin 2020). The plant extract is comprised of polyphenols, flavonoids, etc. in which polyphenols are known to be strong reducers and effective metal chelators forming stable complexes with iron (Ozkan *et al.* 2018). Iron also possesses octahedral geometry, could coordinate upto three polyphenol groups (Yu *et al.* 2018). However, green iron particles are evolving and there is no adequate study to comprehend their competence on reactive dyes (widely used on cotton fabrics) decolorization.

In this study, the bare iron (B-nZVI) and green iron particles (GT-nZVI and GP-nZVI) were synthesized and utilized for the decolorization study of reactive dyes such as reactive red 195 (RR), reactive yellow 145 (RY), reactive blue 4 (RB), reactive black 5 (RBB). The green iron particles were synthesized using green tea leaves extract (GT-nZVI) and grape leaves extract (GP-nZVI). The synthesized particles were characterized for size, crystal structure, morphology, elements; functional groups attached and BET specific surface area. The dye decolorization was examined and the parametric study was conducted. The reaction kinetics and adsorption isotherm of iron particles were investigated. The intermediate products were monitored and the respective decolorization pathway was proposed. Then, the competence of green iron particles on real textile wastewater treatment was examined and reported.

MATERIALS AND METHODS

Chemicals and stock solution

Sodium borohydride ($NaBH_4$), ferric chloride ($FeCl_3$), hydrochloric acid, ethanol, sodium hydroxide, methanol were all purchased from Merck Private Ltd. Reactive textile dyes such as reactive red 195 ($C_{31}H_{19}ClN_7Na_5O_{19}S_6$), reactive yellow 145 ($C_{28}H_{20}ClN_9Na_4O_{16}S_5$), reactive blue 4 ($C_{23}H_{13}Cl_2N_6O_8S_2$), reactive black 5 ($C_{26}H_{21}N_5Na_4O_{19}S_6$) were purchased from the textile dyeing industries at Tiruppur, Tamil Nadu. The chemical structure of all purchased dyes is shown in Figure 1. The maximum wavelength (λ_{max}) and molecular weight for dyes are presented in Table 1. All the chemicals were of analytical grade and utilized as received without any further purification. The stock solution of 1,000 mg/L of RR, RY, RB, RBB were prepared by dissolving 1 g of each dye in 1 L of distilled water and serial dilutions were made as required from stock solutions. The standard calibration curves of various known concentrations of all dyes for maximum wavelength (λ_{max}) were prepared using UV-Vis spectrophotometer (Jasco Inc., Japan) and it was utilized to determine unknown dye concentration.

Synthesizing and characterization of bare and green iron particles

The bare iron particles (B-nZVI) were synthesized by sodium borohydride method (Raman & Kanmani 2019) and green iron particles using green tea leaves extract (GT-nZVI) and were synthesized as discussed in an earlier study (Raman & Kanmani 2018). The synthesizing approach of green iron particles using grapes leaves extract (GP-nZVI) is presented in Figure 2. The leaves of *Vitis vinifera* (black grapes) were collected, washed with deionized water, then dried under shade for 15–20 days and finely powdered. 250 mL of methanol was added to 5 g of the powder and the extract was vacuum filtered after an hour. The extract was then treated with 0.5M $FeCl_3$ at a volumetric ratio of 1:1. An intense black precipitate confirmed the formation of GP-nZVI. It was vacuum filtered, dried and kept in a desiccator until further use.

The particle size was observed based on dynamic light scattering technique using nano particle analyzer SZ-100

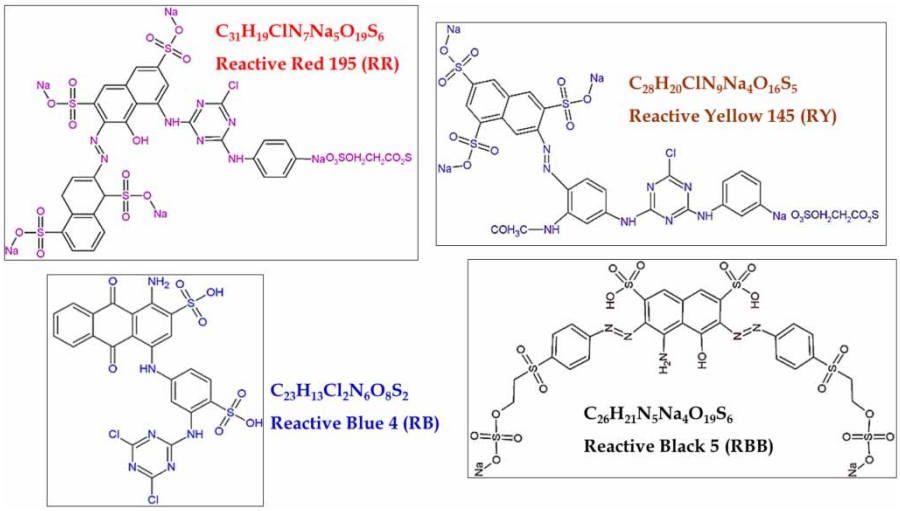

Figure 1 | Chemical structure of dyes.

Table 1 | Particulars of dyes

Dye	λ_{max} (nm)	Molecular Weight (g/mol)
Reactive Red 195 (RR)	542	1,136.32
Reactive Yellow 145 (RY)	418	1,026.25
Reactive Blue 4 (RB)	597	636.43
Reactive Black 5 (RBB)	597	991.789

(Horiba, Japan). The crystal structure was examined using Ultima-IV X-ray diffractometer (Rigaku, Japan) with Cu Kα radiation. The operating voltage and current was maintained at 40 kV and 30 mA. The reflections were scanned from 2θ of 5° to 100° at a rate of 5° per minute with a step size of 0.02°. The size, morphology, and the elemental analysis were studied using transmission electron microscopy (TEM) coupled with energy-dispersive X-ray spectroscopy (EDS), which was acquired using Tecnai G2 Spirit (FEI, The Netherlands). The TEM images of different magnifications were recorded. Fourier transform infra-red (FTIR) spectrum of fresh and used iron particles were recorded using Perkin–Elmer (Instrument Co. Ltd, USA). The Brunauer–Emmett–Teller (BET) specific surface area of three synthesized iron particles was measured based on BET-N_2 adsorption method using Micromeritics ASAP 2020 (Micromeritics, USA).

Decolorization experiment

The decolorization experiments were conducted on 50 mL of RR, RY, RB, and RBB dye solution in which B-nZVI, GT-nZVI and GP-nZVI particles were added. An aliquot of 5 mL was collected at every 2, 4, 6, 8, 10, 15, 30, 60 min and centrifuged. The absorbance of the residual dye in the centrifugate was measured using UV-Vis spectrophotometer. After observing the dye concentration, the sample was analyzed for COD using open reflux method. The effect of iron dose (0.4–1.8 g/L), initial dye concentration (25–200 mg/L) and pH (3–11) on maximum dye removal was studied. The dye concentration range was fixed based on mass balance study conducted with dyebath wastewater samples. The amount of dye adsorbed (mg/g) at equilibrium (q_e) and (q_t) at any time t was calculated using Equations (1) and (2).

$$q_e = \frac{(C_0 - C_e)V_d}{W_i} \tag{1}$$

$$q_t = \frac{(C_0 - C_t)V_d}{W_i} \tag{2}$$

where C_0, C_e, C_t are the dye concentration in the solution initially, at equilibrium, and at any time respectively; V_d is the volume of the dye solution (L) and W_i the mass of nano iron used (g). Control experiment was performed by adding individually ferric chloride solution, sodium borohydride solution, green tea leaves extract, grape leaves extract to all dyes in order to understand their influence on dye decolorization. The repeatability of the experiment confirms the precision of results. Hence, all the dye decolorization experiments were performed in triplicate and obtained the results with a standard deviation error of less than 5%. At an optimized condition, when the maximum decolorization

Figure 2 | Synthesis of green iron particles (GP-nZVI).

was observed, the concentrate of the decolorized solution was collected using a rotary evaporator. Ethanol was utilized to preserve the residue and gas chromatography – mass spectrometry (GC-MS) QP 2010 plus (Shimadzu, Japan) was used to analyze the residue. The intermediate products were identified based on GC-MS and the dye decolorization pathway was proposed.

Reaction kinetics and adsorption isotherm

The dye color removal kinetics were investigated using Lagergren first order model (Lagergren 1898), pseudo-second-order model (Ho & McKay 1999) and the respective reaction rate Equations (3) and (4) are as follows:

$$\frac{t}{q_t} = \frac{1}{k_2 q_e^2} + \frac{t}{q_e} \tag{3}$$

$$\log(q_e - q_t) = \log q_e - \frac{k_1 t}{2.303} \tag{4}$$

where k_1 is the rate constant (1/min) of pseudo-first-order reaction, k_2 is the pseudo-second-order rate constant (g/(mg.min)). The values of k_1 and q_e could be obtained from the plot of $\log(q_e - q_t)$ versus t and the value of k_2 could be calculated from the plot of t/q_t versus t. The Langmuir and Freundlich adsorption isotherm models (Freundlich 1907; Langmuir 1918) were studied to analyze the experimental data using Equations (5) and (6).

$$\frac{C_e}{q_e} = \frac{C_e}{q_m} + \frac{1}{q_m K_L} \tag{5}$$

$$\log q_e = \log K_F + \frac{1}{n} \log C_e \tag{6}$$

where K_L (L/mg), K_F ((mg/g) (L/mg)$^{1/n}$) are the Langmuir and Freundlich adsorption constants and q_m is the maximum adsorption capacity (mg/g) of nano iron particles. The Langmuir isotherm is based on the assumptions of homogenous adsorption surface and includes monolayer physical adsorption, whereas the Freundlich isotherm assumes a multilayer sorption onto heterogeneous surface of adsorbent. The values of q_m and K_L were calculated using a plot between C_e/q_e and C_e. Similarly, the values of n and K_F were obtained from the plot of $\log q_e$ versus $\log C_e$. An indication of degree of the molecular interactions in the adsorbed phase is provided by a parameter called the separation factor R_L which is used to describe the essential characteristics of Langmuir isotherm. The separation factor (R_L) could be calculated using Langmuir constant K_L as in

Equation (7).

$$R_L = \frac{1}{1 + K_L C_o} \quad (7)$$

The separation factor R_L indicates the nature and the feasibility of the adsorption process.

RESULTS AND DISCUSSION

Characterization of synthesized iron particles

The bare and green iron particles synthesized were characterized for size, shape, elemental composition, crystal structure, specific surface area and functional groups attached. The average particle size was 20–80 nm for bare iron and 120–160 nm for green iron respectively (Figure S1, supplementary data). In recent studies (Fan *et al.* 2009; Rahman *et al.* 2014; Sohrabi *et al.* 2016), the bare iron size was reported similarly as less than 100 nm, whereas the green iron size was reported as 172 nm (Gao *et al.* 2016). The morphology of B-nZVI is spherical and due to its magnetic property, with respect to time, a chain-like structure was observed (Figure S2); however, GT-nZVI and GP-nZVI showed irregular clusters of biomolecules capping individual iron particles (Figure S2 and Figure 3). The TEM images of green iron confirm the prevention of aggregation of iron by polyphenolic compounds and same pattern was reported earlier in a study (Hoag *et al.* 2009). The EDS revealed the presence of high carbon and oxygen content in green iron due to polyphenolic compounds.

The XRD spectrum of B-nZVI spectrum showed peaks at 2θ of 45°, 65.8°, 81.8° which confirmed the existence of body centered cubic crystal of iron and respective miller indices were 110, 200, and 211 ((Fan *et al.* 2009). In addition, the peak at 2θ of 35.5° and 62.7° indicated the formation of oxide layers (Fe_3O_4 and Fe_2O_3) on the bare surface as a signal of oxidation (Figure S3). As the morphology of green iron was amorphous in nature due to the preferred orientation of iron particles with the polyphenolic compounds, the XRD showed no peaks along 2θ both for GT-nZVI (Figure S4) and GP-nZVI (Figure 3), respectively, and similar observations for green iron were reported recently (Huang *et al.* 2014).

The FTIR spectrum (Figure 3) of B-nZVI showed a small peak at 542 cm^{-1} and this may be due to the formation of oxide layers on the iron surface when exposed to atmospheric oxygen. The FTIR spectra of GT-nZVI and GP-nZVI showed a broad envelope due to OH stretching vibration of 3,600–2,500 cm^{-1} (Huang *et al.* 2014; Luo *et al.* 2015). The broadening is due to hydrogen bonding of OH groups and the sharp peak at 1,606 cm^{-1} and 1,605 cm^{-1} is due to the vibrations of aromatic ring in epigallocatechin gallate and malonylglucoside compounds of GT-nZVI and GP-nZVI respectively (Figure 3). The peaks at 636 cm^{-1} and 643 cm^{-1} in the fingerprint region confirmed the presence of Fe-O bond in GT-nZVI and GP-nZVI. Hence, from this analysis it is confirmed that polyphenolic compounds are largely involved in complexation with Fe^{3+} in green iron and thus amorphous morphology.

The BET surface area of B-nZVI, GT-nZVI and GP-nZVI was found 31.04 m^2/g, 14.6 m^2/g and 15.08 m^2/g respectively and this demonstrates that increase in green iron size showed reduced BET surface area. Increased BET surface area could enhance adsorption process and which is typically high (2,636 m^2/g) for activated carbon, hence maximum adsorption capacity (Kumar & Jena 2016). Earlier studies reported 29–33.5 m^2/g for bare iron (Chen 2005; Chompuchan *et al.* 2009; Shih *et al.* 2010) and 5.8–6.67 m^2/g for green iron (Huang *et al.* 2014; Yu *et al.* 2018). Gao *et al.* (2016) reported 54.27 m^2/g of surface area for 172 nm of green iron, which is objectionable as the increase in particle size automatically reduces specific surface area (Ponder *et al.* 2001; Sun *et al.* 2006). The observed BET surface area confirms the competence of adsorption of bare and green iron but is not as effective as activated carbon.

Reactive dye decolorization

The reaction between dye molecules and the iron particles (B-nZVI, GT-nZVI, and GP-nZVI) were studied by varying iron dose (0.4–2.6 g/L), dye concentration (25–200 mg/L) and pH (3–11). The reactive dyes RR, RY, RB, and RBB have different molecular weights and complicated structure, hence the iron dose required for maximum decolorization were varied. The UV-Vis spectra of RR, RY, RB, and RBB before and after treatment with B-nZVI, GT-nZVI, GP-nZVI at optimized dose and 25 mg/L initial dye concentration is presented in Figure 4. The absorbance at λ_{max} of RR (542 nm), RY (418 nm), RB (597 nm), and RBB (597 nm) immediately disappeared within 30 min of treatment with bare and green iron particles. The decolorization efficiency of B-nZVI, GT-nZVI, and GP-nZVI in RR, RY, RB and RBB dyes for 30 min of contact time is illustrated in Figure 5. The decolorization attained close to 90–98% for all the dyes in the presence of bare and green iron particles. The results therefore illustrate the

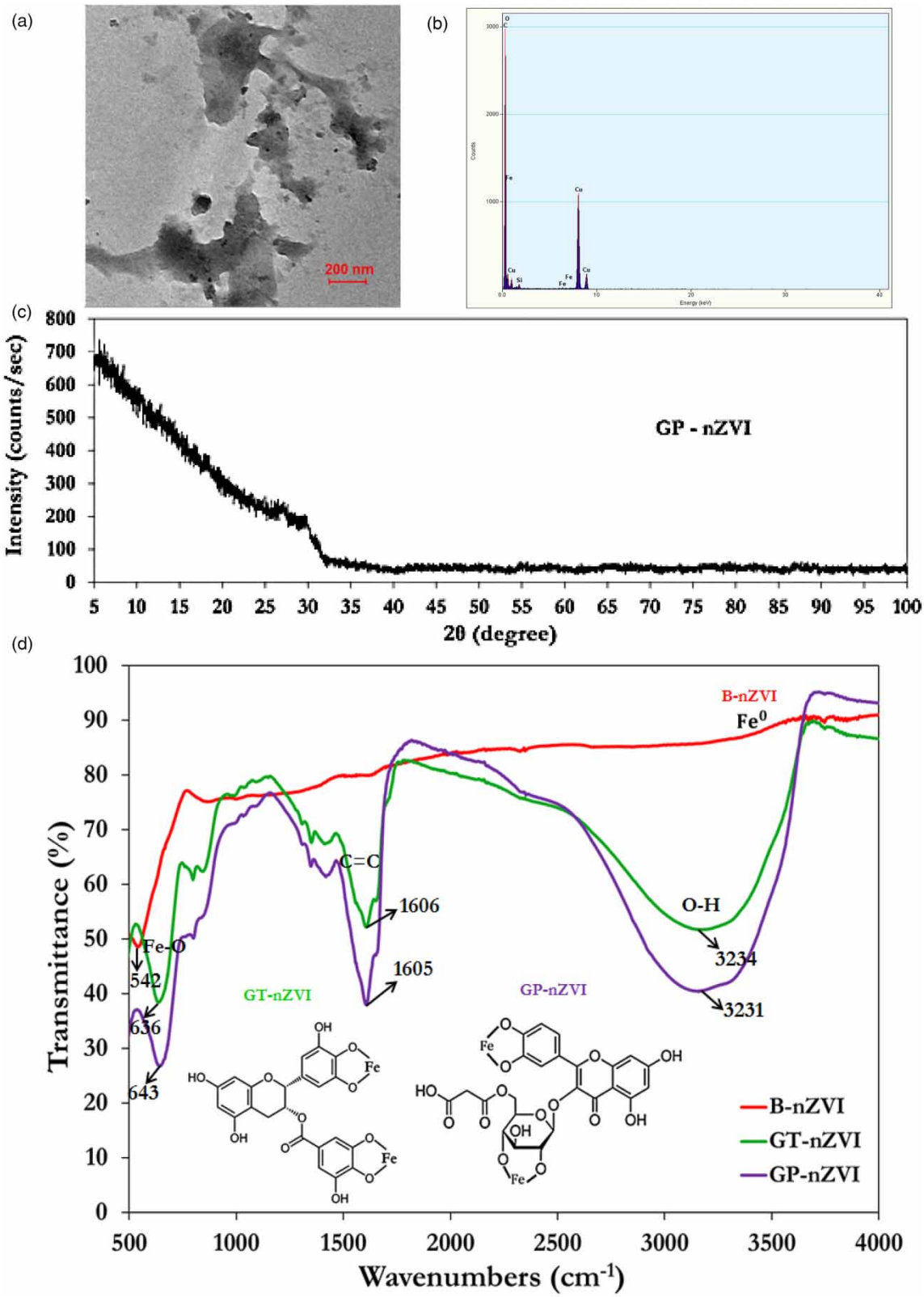

Figure 3 | (a) TEM image (b) EDS (c) X-ray diffraction spectrum of GP-Nzvi. (d) FTIR spectra of freshly synthesized iron particles.

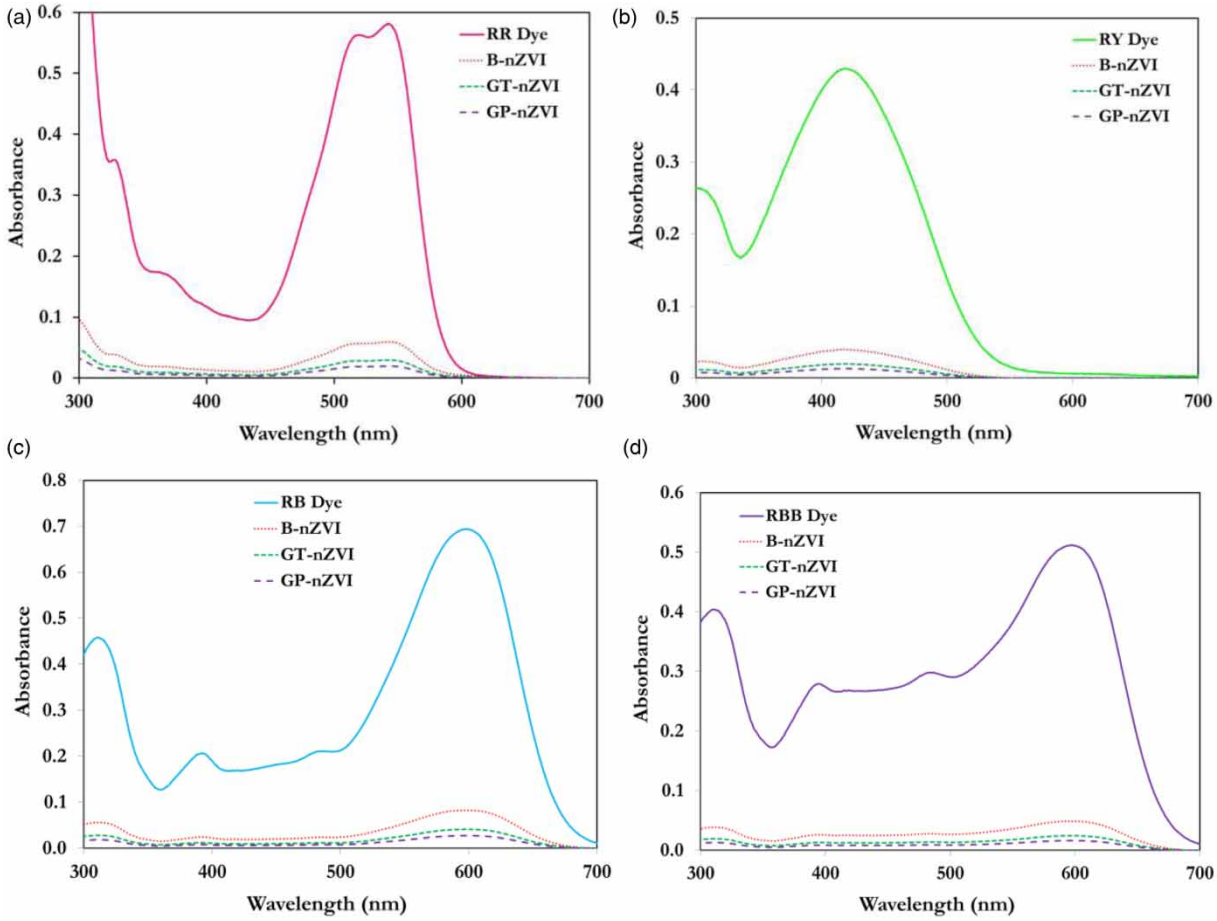

Figure 4 | UV-Vis spectra of (a) RR (b) RY (c) RB and (d) RBB before and after treatment.

versatility of iron particles for treatment of textile dyeing wastewater.

The decolorization process was almost finished within 15 min of contact time. The ferric chloride solution, sodium borohydride solution, *Camellia sinensis* leaves extract and *Vitis vinifera* leaves extract were added to all dyes individually. The ferric chloride and sodium borohydride showed no influence in the decolorization efficiency and hence it is confirmed that these precursors do not have any role in reactive dye decolorization. Similarly, the components of *Camellia sinensis* and *Vitis vinifera* leaves extract as such are not adequate to decolorize any dyes. This demonstrates the key role of B-nZVI, GT-nZVI, and GP-nZVI in reactive dye decolorization process. The influence of dye concentration on reactive dye decolorization was studied at optimized dose of bare and green iron and the study was conducted with the initial pH 7 of reactive dyes. The dye concentration was varied as 25, 50, 100, 150, and 200 mg/L for RR, RY, RB, and RBB. GP-nZVI and GT-nZVI decolorized 95–98% whereas B-nZVI decolorized 90–92% of all reactive dye at 25 mg/L concentration; however, the potential of green iron particles in decolorization is reduced to 52% and 49% for RR, 64% and 61% for RY, 78% and 71% for RB, 76% and 68% for RBB at 200 mg/L dye concentration. The bare iron decolorized 46% of RR, 56% of RY, 65% of RB, 62% of RBB at 200 mg/L of dye concentration. It is evident that increase in dye concentration reduced decolorization efficiency of iron particles as all the reactive sites were utilized by dye molecules and there was a demand for more reactive sites of iron. Similarly, Sohrabi *et al.* (2016) reported 95% of Reactive Blue 21 decolorization was achieved at 30 mg/L of initial concentration; however, increase in dye concentration reduced the decolorization efficiency of 0.5 g bare iron particles.

The effect of pH for all reactive dyes of 25 mg/L initial concentration at optimized dose is studied. Slight decrease in dye decolorization efficiency was observed when pH

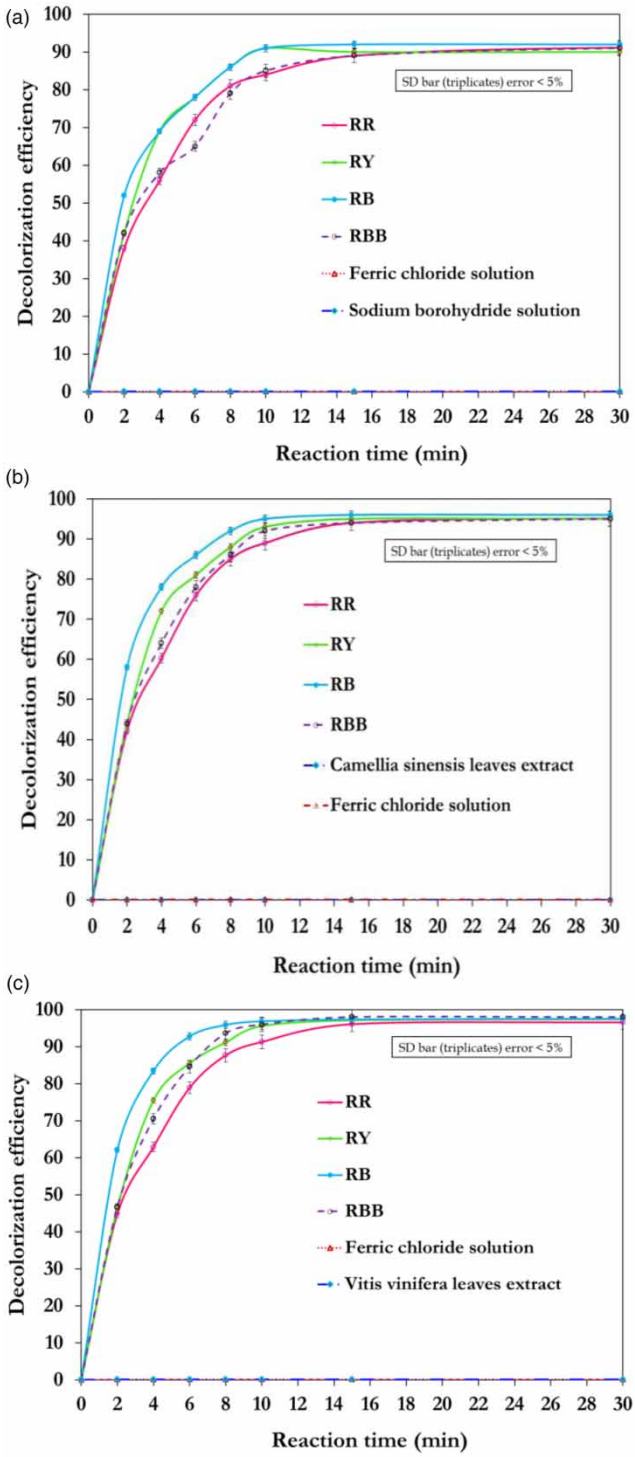

Figure 5 | Decolorization of RR, RY, RB and RBB using (a) B-nZVI (b) GT-nZVI (c) GP-nZVI.

was increased from 3 to 11. Hence, pH has less effect on reactive dye decolorization (Chen *et al.* 2018; Trevizani *et al.* 2018). This was further demonstrated by the point of zero charge (pH 8) studies conducted on the bare and green iron particles. It was found that at higher pH values (above the point of zero charge); the surface of iron acquired a negative surface. All the reactive dyes contain azo groups and protonation of azo groups was expected in the presence of H^+ ions when pH is lower than pH of point of zero charge. Once all the reactive sites of iron particles were utilized by dye molecules, the passive layer of oxides and hydroxides on iron surface induced adsorption. From the results, it is evident that the order of the reactivity of iron particles in dye decolorization is GP-nZVI > GT-nZVI > B-nZVI. Similarly, the order of reactive dyes achieved maximum decolorization at an optimized iron dose is RB > RBB > RY > RR. This might be ascribed to the bulky nature of RR and RY. Increase in iron dose increased the reactive sites for the dye decolorization and once all the sites were utilized by the reactive dye molecules, a greater number of basic nitrogen sites in RR, RY, RB enhanced adsorption with iron particles. Thus, reduction and adsorption processes are involved in the reactive dye decolorization (Huang *et al.* 2014; Luo *et al.* 2015).

Reaction kinetics and adsorption isotherm

The dye decolorization kinetics was investigated using pseudo-first-order and pseudo-second-order models. Pseudo-first-order model is fit better for RY, RBB decolorization using B-nZVI, and then RR, RBB decolorization using GT-nZVI, and RR, RY decolorization using GP-nZVI and the respective rate constants were computed and presented in Table 2. Other decolorization fits well with pseudo-second-order model. The pseudo-first-order and second-order correlations varied less than 5%. The pseudo-first-order fit confirms the reaction between iron particles and dye molecules with rate constant 0.317–0.422 and it is followed by adsorption, which was confirmed with data fit pseudo-second-order model. Similar observations were reported by Chompuchan *et al.* (2009) and Gao *et al.* (2016) for reactive dye decolorization.

The adsorption isotherms were investigated for reactive dye decolorization using bare and green iron particles. From Table 3, it is observed that the correlation of determination R^2 value of Langmuir isotherm model is favorable to experimental data than Freundlich isotherm model. This demonstrates the monolayer adsorption of dye molecules on the homogenous surface of iron was achieved (Lemraski & Tahmasebi 2018). The computed maximum adsorption capacity of bare iron and green iron was 4.704–9.901 mg/g and 11.575–14.749 mg/g, respectively. The adsorption capacity of bare and green iron is low when compared to

Table 2 | Reaction kinetics constants

			First order			Second order		
Iron particles	**Dyes**	**q_e exp. (mg/g)**	**q_e calc. (mg/g)**	**k_1 (1/min)**	**R^2**	**q_e calc. (mg/g)**	**k_2 (g/(mg.min))**	**R^2**
B-nZVI	RR	8.104	7.075	0.406	0.873	9.099	0.041	0.924
	RY	12.039	11.485	0.317	0.954	13.889	0.023	0.898
	RB	14.919	14.591	0.422	0.978	15.748	0.079	0.989
	RBB	15.305	14.722	0.413	0.962	18.018	0.017	0.885
GT-nZVI	RR	10.049	9.828	0.325	0.978	11.038	0.045	0.952
	RY	14.454	13.616	0.357	0.942	16.077	0.028	0.944
	RB	15.586	15.243	0.422	0.978	16.26	0.094	0.993
	RBB	14.999	14.429	0.413	0.962	16.502	0.031	0.957
GP-nZVI	RR	13.414	13.186	0.34	0.983	14.535	0.041	0.969
	RY	16.404	16.256	0.382	0.991	17.637	0.044	0.978
	RB	17.414	17.031	0.422	0.978	18.116	0.089	0.994
	RBB	15.112	14.538	0.413	0.962	16.393	0.047	0.976

Table 3 | Adsorption isotherm constants

			Langmuir constants			Freundlich constants		
Iron particles	**Dyes**	**q_e exp. (mg/g)**	**q_e calc. (mg/g)**	**K_L(L/mg)**	**R^2**	**n**	**K_F (mg/g) (L/mg)$^{1/n}$**	**R^2**
B-nZVI	RR	9.614	4.704	0.316	0.949	2.726	3.433	0.808
	RY	12.712	7.231	0.449	0.965	3.419	3.641	0.775
	RB	14.253	9.901	0.654	0.987	4.717	3.64	0.845
	RBB	12.459	6.658	0.395	0.971	2.777	3.819	0.854
GT-nZVI	RR	11.575	7.485	0.677	0.976	6.083	3.098	0.747
	RY	14.756	10.011	0.949	0.977	7.199	3.38	0.652
	RB	15.587	12.225	1.501	0.993	9.542	3.43	0.759
	RBB	14.488	9.337	0.801	0.982	5.279	3.464	0.776
GP-nZVI	RR	13.414	10.204	1.298	0.988	13.072	3.117	0.663
	RY	16.404	12.136	1.612	0.983	15.129	3.366	0.484
	RB	17.414	14.749	2.935	0.995	19.841	3.476	0.609
	RBB	15.111	10.482	1.277	0.984	8.569	3.307	0.719

activated carbon from coconut shell (51.56–62.06 mg/g). Similar adsorption behavior was observed for methylene blue and vat green dye decolorization using bare iron in previous studies and the adsorption capacity of bare iron was reported as 5.53 mg/g (Arabi *et al.* 2013; Hamdy *et al.* 2018). The n value greater than one indicates physical adsorption process was achieved between dye molecules and iron particles.

The adsorption between reactive dye molecules and iron particles involves electrostatic interactions and which can be either attractive or repellent, based on the surface charge of the dye molecules and iron particles. This is influenced by dye solution pH and confirmed by point of zero charge studies. It was found that at high pH, the surface of iron accumulates negatively charged dye molecules which are repellent in nature, thus decrease in decolorization efficiency. Therefore, electrostatic interactions were part of the adsorption mechanism (Chi *et al.* 2017; Hlekelele *et al.* 2019). The structure of reactive dye molecules consists of aromatic rings with delocalized π electrons; therefore π–π non-electrostatic interactions were also part of the adsorption mechanism. The separation factor R_L value 0.013–0.112 demonstrates that the adsorption of dye molecules on the iron surface is favorable (Hamdy *et al.* 2018).

Identification of intermediates and products

The intermediates and products formed during RR, RY, RB and RBB dye decolorization were determined using GC-MS and the detected molecular ions in the mass spectrum are

presented in Table 4. This provides insight on the underlying decolorization mechanism and the respective decolorization pathway using green iron particles (GP-nZVI) was proposed and presented in Figures 6 and 7. The azo bond present in the parent molecule of RR dye (m/z 1136) was initially broken by B-nZVI (Figure S4) and the compound was reduced to m/z 534 and m/z 334. However, green iron (Figures S4 and 6) reduced the parent molecule m/z 1136 into individual aromatic structures m/z 246, m/z 232, and m/z 214 respectively. Especially, GP-nZVI demonstrated RR decolorization into smaller molecular compounds compared to GT-nZVI, thus the decolorization efficiency order GP-nZVI > GT-nZVI > B-nZVI was observed. Most of the degraded products are aromatic structures and no azo bond was perceived, hence the complete decolorization of RR dye was observed. Benzene, phenyl sodium, 2-chloro-1,3,5-triazine, di hydro naphthalene, sodium benzene sulfonate, methyl cyclo hex enol were the major intermediates observed in RR decolorization using bare and green iron particles. The azo bond and the weak –NH– bonds present in the parent molecule of RY dye (m/z 1026) were initially broken and the compound was reduced to m/z 434, m/z 230 and m/z 229 in the presence of B-nZVI (Figure S5). However, green iron reduced the parent molecule m/z 1026 into smaller aromatic structures m/z 128, m/z 115, m/z 108, m/z 100, m/z 93 and m/z 78 (Figures S5 and 6). Hence, the decolorization efficiency of green iron particles is better than bare iron. Intermediates and products such as naphthalene, 2-chloro-1,3,5-triazine, benzene 1,2 di amine, phenyl sodium, aniline and benzene were observed in RY decolorization using bare and green iron particles.

The weak –NH– bonds present in the parent molecule of RB dye (m/z 636) were initially broken and the compound was reduced to m/z 288, m/z 158 and m/z 150 in the presence of B-nZVI (Figure S6). However, green iron reduced the parent molecule m/z 636 into smaller aromatic structures m/z 223, m/z 208, m/z 158, m/z 115, and m/z 93 respectively (Figures S6 and 7). Naphthalene, 2-chloro-1 3,5-triazine, anthracene-9,10 dione, 1,3,5 triazine, aniline and benzene were the intermediates and products observed during RB decolorization using bare and green iron particles. The azo bonds present in the parent molecule RBB (m/z 992) were initially broken and the compound was reduced to m/z 159, m/z 158 and m/z 128 in the presence of B-nZVI (Figure S7). However, green iron reduced the parent molecule m/z 636 was further degraded into smaller aromatic structures m/z 110, m/z 94, m/z 86, and m/z 78, and m/z 93 respectively (Figures S7 and 7). Naphthalene, aniline, benzene, phenol, naphthalene-1-amine, benzene sulfonic acid and benzene-1, 3-di ol, hexane were the intermediates and products observed during RBB decolorization using bare and green iron particles. Thus, the green iron could disintegrate RB and RBB dye molecules into lower compounds better than bare iron. This confirms not only adsorption but also reduction process are involved in the reactive dye decolorization (Huang *et al.* 2014; Luo *et al.* 2015).

Decolorization mechanism of green iron particles

The green iron forms chelate bond with polyphenolic compounds and the bonds were dissolved once the green iron particles are released into dye solution and iron acts as zero valent instantly. Then, the zero valent iron is oxidized to ferrous ion, and then undergoes further oxidative transformation to ferric ion. The oxidation process emitted enormous amount of electrons, those involved in the reaction. The ferric ions in the presence of water forms ferric hydroxide and generate hydronium (H^+) ions. The emitted electrons are accepted by the dye molecules and thereby dye molecules were reduced and intermediates, products were formed. Further reactions of bare iron with atmospheric dissolved oxygen and water generate hydrogen

Table 4 | Detected molecular ions during dye decolorization

Iron particles	Molecular ions (m/z) from mass spectrum			
	RR dye	RY dye	RB dye	RBB dye
B-nZVI	534, 334, 214, 180, 116, 115, 100	434, 230, 229, 128, 115, 108, 100, 93, 78	288, 208, 158, 150, 128, 115, 93, 78	159, 158, 143, 128, 93, 78
GT-nZVI	246, 232, 214, 180, 130, 116, 112, 100, 78	230, 229, 128, 115, 108, 100, 93, 78	223, 208, 158, 128, 115, 81, 78	159, 158, 143, 128, 124, 110, 94, 93, 78
GP-nZVI	232, 214, 180, 130, 144, 116, 112, 100, 78	230, 128, 115, 108, 100, 93, 78	208, 158, 128, 115, 93, 81, 78	180, 159, 158, 144, 143, 128, 94, 93, 86, 78

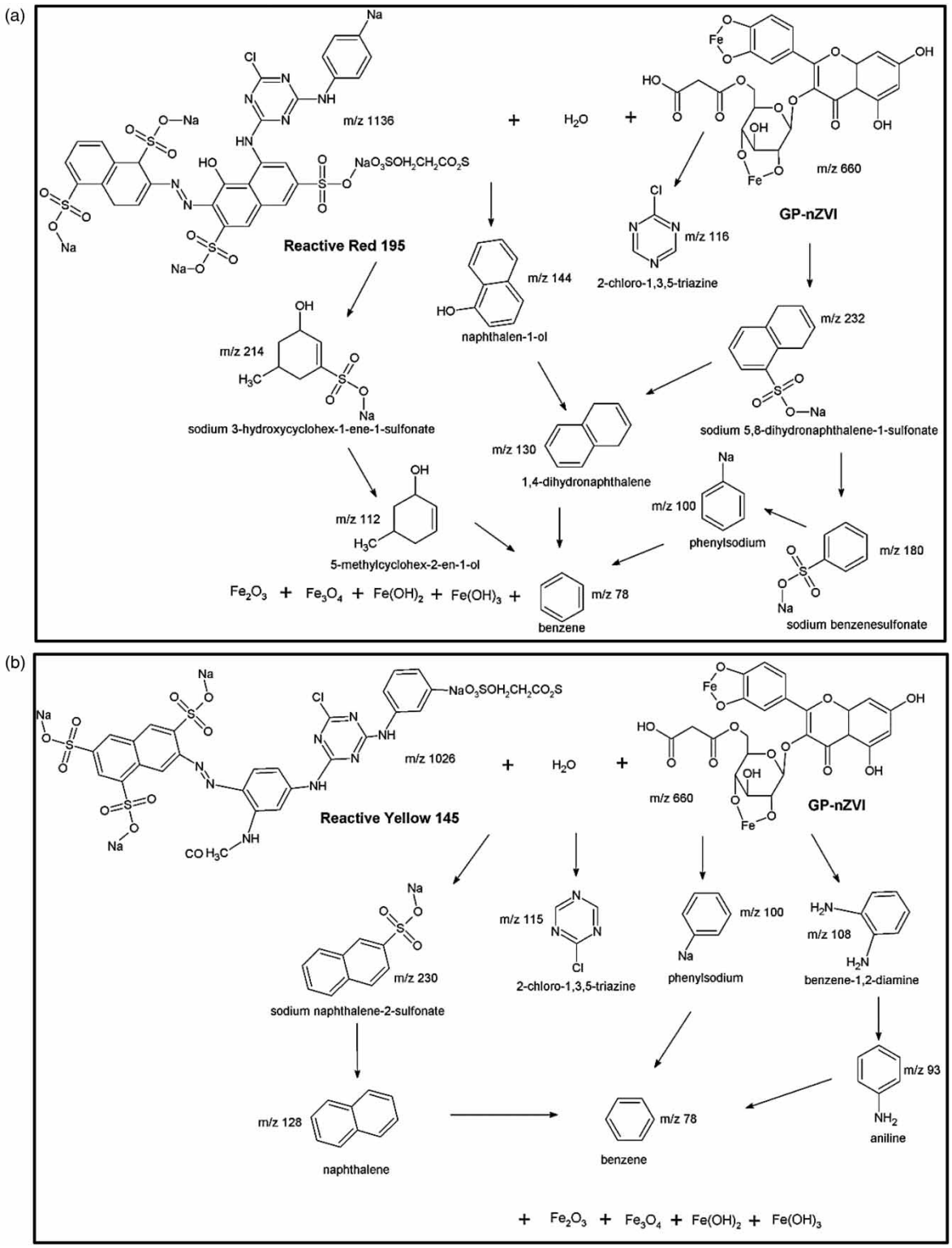

Figure 6 | Proposed (a) RR dye and (b) RY dye decolorization pathway using GP-nZVI.

peroxide (Donadelli *et al.* 2018). Similarly, the generated electrons in the presence of H^+ ions also react with dissolved oxygen and produce hydrogen peroxide. Ferrous ions catalyze hydrogen peroxide and generate hydroxyl radicals (Wu *et al.* 2014), which in turn react with dye molecules and metabolites are formed. In addition, the electrostatic

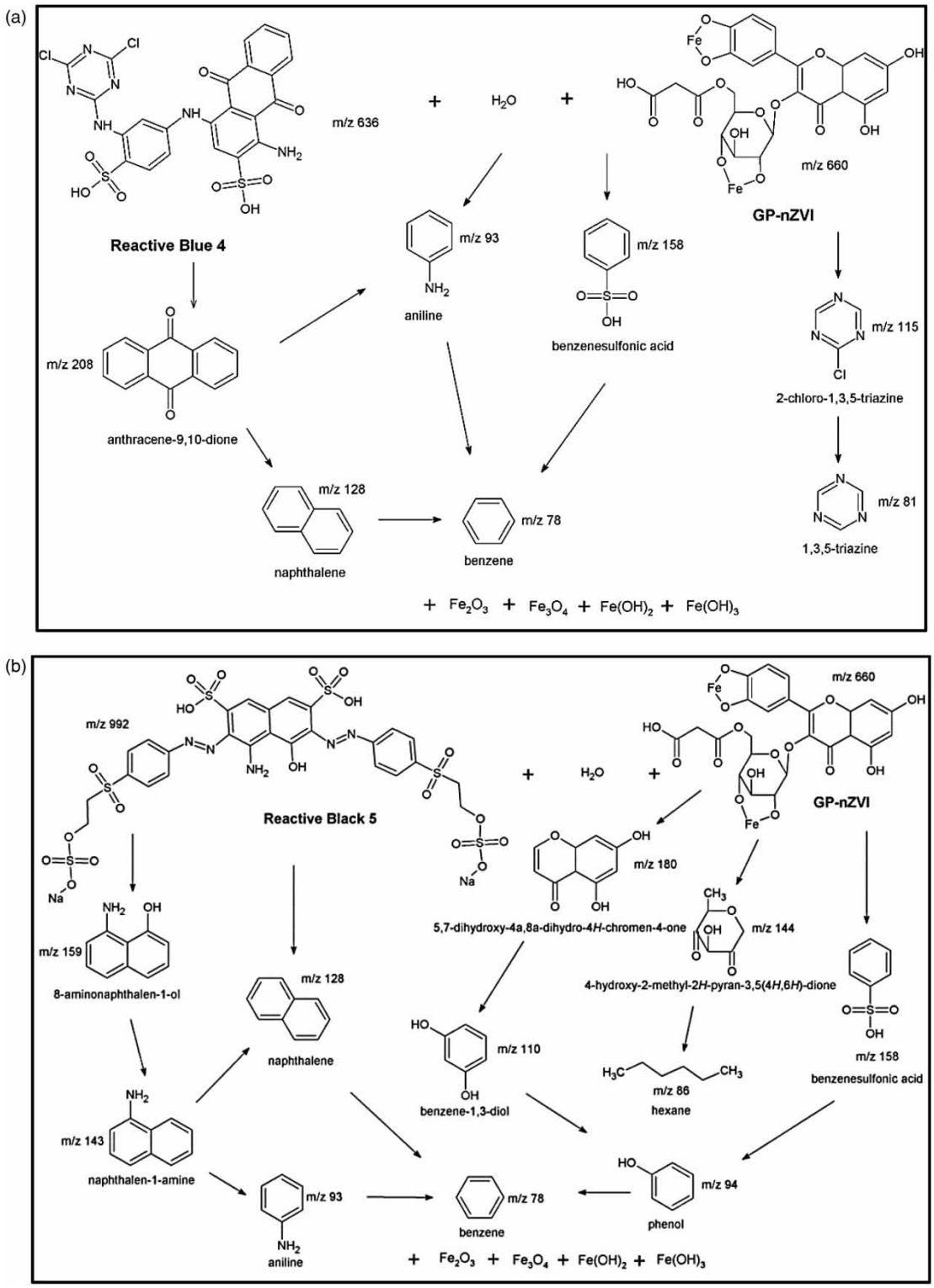

Figure 7 | Proposed (a) RB dye and (b) RBB dye decolorization pathway using GP-nZVI.

interaction between dye molecules and iron particles, π–π non-electrostatic interaction are also involved in the adsorption process. The ferrous and ferric ions are converted into ferric hydroxides and could also be involved in physical adsorption of dye molecules and metabolites (Mu *et al.* 2017).

Figure 8 | Decolorization of textile wastewater by bare and green iron particles.

The FTIR spectrum of used bare and green iron particles is presented in Figure S8. The spectrum of B-nZVI showed peaks at 1,021 cm^{-1}, 828 cm^{-1}, and 820 cm^{-1}, thus confirming hydroxide layers on the iron surface. Also, the small peaks observed at 546 cm^{-1}, 656 cm^{-1}, and 660 cm^{-1} represented the existence of oxide layers on the iron surface, those were exposed to oxidation and reduction during reaction. All the strong and broad C-OH, C=C, O-H bonds observed due to polyphenolic compounds in freshly synthesized green iron (Figure 3) were diminished after use (Figure S8). A similar observation was reported (Shahwan *et al.* 2011) for methyl orange dye decolorization using green iron particles synthesized from green tea leaves extract. The disappearance of polyphenolic groups from used green iron particles confirmed the dissociation of polyphenolic compounds during dye decolorization.

Textile wastewater treatment

The performance assessment of green iron particles on real textile wastewater treatment is required before it is opted for any industrial applications. The wastewater consists of mixture of reactive dyes, inorganic salts and it is a combined wastewater from the pretreatment, dyeing and rinsing process. Five samples of textile wastewater (TWW1, TWW2, TWW3, TWW4, and TWW5) were collected (Figure 8) and analyzed for pH, electrical conductivity (EC), total dissolved solids (TDS), chlorides (Cl), sulphates (SO_4), sodium (Na), chemical oxygen demand (COD), and total organic carbon (TOC). The characterized results are summarized in Table 5, which confirms the presence of organics due to textile dyes and high inorganic salts. The wastewater was scanned at multiple wavelengths of 436, 525, 620 nm (ISO 7887: 1985) after removing the turbidity by centrifugation for color measurement as the wastewater contains more than one reactive dye and no single peak was observed.

Table 5 | Characterization of collected textile wastewater

Parameters	TWW1	TWW2	TWW3	TWW4	TWW5
pH	8.97	9.04	10.20	8.80	8.68
EC (dS/m)	19.07	14.19	2.73	23.30	16.14
TDS (mg/L)	9,728	7,095	1,543	11,670	9,119
COD (mg/L)	1,640	1,240	920	820	1,268
TOC (mg/L)	566	428	314	283	437
Cl (mg/L)	6,613	3,630	241	8,588	4,582
SO_4 (mg/L)	580	460	94	1,190	679
Na (mg/L)	4,562	1,258	156	5,330	2,508

The bare and green iron dose of 2 g/L was utilized for the treatment of textile wastewater. The decolorization of wastewater was monitored at every 5, 10, 15, 30, and 60 min. Although the equilibrium was attained in 30 min of contact time, to ensure steady state, the reaction was monitored until 60 min. The pH 8.68–10.2 of textile wastewater was reduced to 7.4–8.2 and 7.2–7.6 in the presence of bare and green iron respectively. The decolorization efficiency of B-nZVI was 72–82%. However, GT-nZVI decolorized 80–89% whereas GP-nZVI decolorized 83–92% of textile wastewater (Figure 8). Bare iron removed only 19–32% of COD; however, GT-nZVI and GP-nZVI removed 35–48% and 43–52% of COD respectively (Table 6). This demonstrates that the reactivity of green iron is better than bare iron and the order of reactivity is GP-nZVI > GT-nZVI > B-nZVI. It is significant to discuss the reduction observed in the quantity of inorganic salts (Cl, SO_4, and Na) during the treatment. The reduction was less than 10% using B-nZVI and it was around 12% for GT-nZVI and 14% for GP-nZVI. This might be due to the adsorption of inorganic salts on the oxidized iron surface.

The cost for textile wastewater treatment using bare and green iron particles were computed based on the chemicals utilized for synthesis. This confirms that textile wastewater treatment using GT-nZVI (0.18 $/$m^3$) and GP-nZVI (0.29 $/$m^3$) was found to be very cheap compared to B-nZVI (2.32$/$m^3$). The estimated cost of the proposed textile wastewater treatment technique is compared with the existing treatment technologies (Table 7) and observed to be economical. As the reactivity of GP-nZVI is also better than other iron particles, it is highly recommended to use the green iron particles from grape leaves in order to decolorize textile wastewater effectively.

Conclusions and future perspectives

1.4–2.0 g/L of green iron decolorized 95–98% of RR, RY, RB, RBB dye at 25 mg/L concentration. However, the potential of green iron particles (GT-nZVI and GP-nZVI) in decolorization is reduced to 52% and 49% for RR, 64% and 61% for RY, 78% and 71% for RB, 76% and 68% for RBB at 200 mg/L dye concentration. Increase in green iron dose increased the reactive sites for dye decolorization, and once all the reactive sites were utilized by the dye molecules, basic nitrogen sites in RR, RY, RBB, and RB as well the oxidized iron surface enhanced adsorption process. The adsorption isotherms fit with Langmuir isotherm model and this demonstrates the monolayer physical adsorption of dye molecules on the homogenous iron surface. Thus the

Table 6 | Characterization of textile wastewater after treatment with bare and green iron particles

	B-nZVI					GT-nZVI					GP-nZVI				
Parameters	TWW1	TWW2	TWW3	TWW4	TWW5	TWW1	TWW2	TWW3	TWW4	TWW5	TWW1	TWW2	TWW3	TWW4	TWW5
pH	7.6	7.4	7.4	8.2	7.8	7.2	7.2	7.2	7.6	7.4	7.2	7.2	7.2	7.6	7.4
EC (dS/m)	18.23	13.53	2.45	22.86	15.29	17.90	13.36	2.40	22.72	15.22	17.57	13.15	2.36	22.62	15.15
TDS (mg/L)	9,256	6,516	1,442	11,124	8,562	9,025	6,412	1,398	10,654	8,512	8,874	6,212	1,366	10,265	8,463
COD (mg/L)	1,158	971	667	559	1,023	934	726	534	426	684	846	632	495	414	608
TOC (mg/L)	284	212	156	127	235	382	264	313	168	241	256	227	208	175	248
Cl (mg/L)	6,512	3,528	225	8,326	4,251	6,417	3,415	214	8,267	4,165	6,315	3,321	214	8,112	4,137
SO_4 (mg/L)	524	414	92	1,145	612	517	408	88	1,126	597	512	398	86	1,108	584
Na (mg/L)	4,313	1,146	146	5,266	2,447	4,298	1,134	142	5,183	2,394	4,242	1,122	145	5,117	2,368

Table 7 | Cost comparison in textile wastewater treatment

Textile Wastewater Treatment	Cost	References
GT-nZVI treatment	0.18 $/m^3	This study
GP-nZVI treatment	0.29 $/m^3	This study
Chemical coagulation	0.35–0.96 $/m^3	Dalvand *et al.* (2011)
Ultrafiltration, Nanofiltration, Reverse osmosis	2.16 $/m^3	Vergili *et al.* (2012)
B-nZVI treatment	2.32 $/m^3	This study
Fenton, fenton integrated with activated sludge, biological, electro coagulation, ion exchange	0.4–3.5 $/m^3	Holkar *et al.* (2016); Yuksel *et al.* (2012)
Ozonation, ozonation and H_2O_2, ozonation and ultra violet, ozonation and biological, H_2O_2 and biological	1.4–5.02 $/m^3	

reduction and adsorption processes are involved in the dye decolorization. Aromatic compounds were detected as intermediates/products and the respective decolorization pathway was proposed. The green iron of 2 g/L dose was optimized for textile wastewater treatment and the decolorization efficiency was 83–92% (GP-nZVI). The pH 8.68–10.2 of textile wastewater was reduced to 7.2–7.6 and 43–52% of COD was removed. This demonstrates that the performance of green iron (GP-nZVI) is remarkable for textile wastewater treatment and found to be economical. The organic residue from green iron has high biocompatibility and, after treatment managing, the residue would be an ecofriendly practice. This study confirms the competence of green iron particles synthesized from grape leaves in reactive dye decolorization and further recommendation to textile wastewater treatment.

ACKNOWLEDGEMENTS

The authors would like to acknowledge the Nano Science & Technology Department of Tamil Nadu Agricultural University, Coimbatore, the Department of Energy Environment, National Institute of Technology, Tiruchirappalli and the Council of Scientific and Industrial Research – National Metallurgical Laboratory, Chennai to provide the characterization facilities for the bare and green iron particles. The authors also would like to thank the Research Centre,

Sathyabama University, Chennai and the Department of Biotechnology, Periyar Maniammai University, Tanjavore, to provide the characterization facilities for reactive dye and textile wastewater samples.

CONFLICT OF INTEREST

We declare that there is no conflict of interest concerning this publication.

DATA AVAILABILITY STATEMENT

All relevant data are included in the paper or its Supplementary Information.

REFERENCES

Arabi, S., Sohrabi, M. R. & Khosravi, M. 2013 Adsorption kinetics and thermodynamics of vat dye onto nano zero-valent iron. *Indian Journal of Chemical Technology* **20** (3), 173–179.

Bhuiyan, M. S. H., Miah, M. Y., Paul, S. C., Aka, T. D., Saha, O., Rahaman, M. M., Sharif, M. J. I., Habiba, O. & Ashaduzzaman, M. 2020 Green synthesis of iron oxide nanoparticle using Carica papaya leaf extract: application for photocatalytic degradation of remazol yellow RR dye and antibacterial activity. *Heliyon* **6** (8), e04603.

Chen, S. Y. 2005 *Discoloration and Degradation of azo Dyes by Nanoscale Iron Particles*.

Chen, J., Xiaohui, W., Hao, W. & Qi, J. 2018 Study on decolorization of dyeing wastewater by electrochemical treatment. *IOP Conference Series: Earth and Environmental Science* **113**, 1–10.

Chi, Z., Wang, Z., Chu, H., Bin, P. & Lucian, L. 2017 Bentonite-supported nanoscale zero-valent iron granulated electrodes for industrial wastewater remediation. *RSC Advances* **7** (70), 44605–44613.

Chompuchan, C., Satapanajaru, T., Suntornchot, P. & Pengthamkeerati, P. 2009 Decolorization of reactive black 5 and reactive red 198 using nanoscale zerovalent iron. *World Academy of Science, Engineering and Technology, International Journal of Chemical and Molecular Engineering* **3** (1), 5.

Corcoran, E., Nellemann, C., Baker, E., Bos, R., Osborn, D. & Savelli, H. 2010 *Sick Water? The Central Role of Wastewater Management in Sustainable Development – A Rapid Response Assessment*. UN-Habitat, Kenya.

Dalvand, A., Gholami, M., Joneidi, A. & Mahmoodi, N. M. 2011 Dye removal, energy consumption and operating cost of electrocoagulation of textile wastewater as a clean process. *CLEAN – Soil, Air, Water* **39** (7), 665–672.

Donadelli, J. A., Carlos, L., Arques, A. & García Einschlag, F. S. 2018 Kinetic and mechanistic analysis of azo dyes decolorization by ZVI-assisted Fenton systems: pH-dependent shift in the contributions of reductive and oxidative transformation pathways. *Applied Catalysis B: Environmental* **231**, 51–61.

Fan, J., Guo, Y., Wang, J. & Fan, M. 2009 Rapid decolorization of azo dye methyl orange in aqueous solution by nanoscale zerovalent iron particles. *Journal of Hazardous Materials* **166** (2–3), 904–910.

Freundlich, H. 1907 Über die Adsorption in Lösungen. *Zeitschrift für Physikalische Chemie* **57U**, 385–470.

Fu, F., Dionysiou, D. D. & Liu, H. 2014 The use of zero-valent iron for groundwater remediation and wastewater treatment: a review. *Journal of Hazardous Materials* **267**, 194–205.

Gao, J.-F., Li, H.-Y., Pan, K.-L. & Si, C.-Y. 2016 Green synthesis of nanoscale zero-valent iron using a grape seed extract as a stabilizing agent and the application for quick decolorization of azo and anthraquinone dyes. *RSC Advances* **6** (27), 22526–22537.

Ghaly, A. E., Ananthashankar, R., Alhattab, M. & R, V. V. 2014 Production, characterization and treatment of textile effluents: a critical review. *Journal of Chemical Engineering & Process Technology* **5** (1), 1–18.

Hamdy, A., Mostafa, M. K. & Nasr, M. 2018 Zero-valent iron nanoparticles for methylene blue removal from aqueous solutions and textile wastewater treatment, with cost estimation. *Water Science and Technology* **78** (2), 367–378.

Hlekelele, L., Nomadolo, N. E., Setshedi, K. Z., Mofokeng, L. E., Chetty, A. & Chauke, V. P. 2019 Synthesis and characterization of polyaniline, polypyrrole and zero-valent iron-based materials for the adsorptive and oxidative removal of bisphenol-A from aqueous solution. *RSC Advances* **9** (25), 14531–14543.

Ho, Y. S. & McKay, G. 1999 Pseudo-second order model for sorption processes. *Process Biochemistry* **34** (5), 451–465.

Hoag, G. E., Collins, J. B., Holcomb, J. L., Hoag, J. R., Nadagouda, M. N. & Varma, R. S. 2009 Degradation of bromothymol blue by 'greener' nano-scale zero-valent iron synthesized using tea polyphenols. *Journal of Materials Chemistry* **19** (45), 8671–8677.

Holkar, C. R., Jadhav, A. J., Pinjari, D. V., Mahamuni, N. M. & Pandit, A. B. 2016 A critical review on textile wastewater treatments: possible approaches. *Journal of Environmental Management* **182**, 351–366.

Huang, L., Weng, X., Chen, Z., Megharaj, M. & Naidu, R. 2014 Green synthesis of iron nanoparticles by various tea extracts: comparative study of the reactivity. *Spectrochimica Acta. Part A, Molecular and Biomolecular Spectroscopy* **130**, 295–301.

Hynes, N. R. J., Kumar, J. S., Kamyab, H., Sujana, J. A. J., Al-Khashman, O. A., Kuslu, Y., Ene, A. & Suresh Kumar, B. 2020 Modern enabling techniques and adsorbents based dye removal with sustainability concerns in textile industrial sector -A comprehensive review. *Journal of Cleaner Production* **272**, 122636.

Kumar, A. & Jena, H. M. 2016 Preparation and characterization of high surface area activated carbon from Fox nut (Euryale ferox) shell by chemical activation with H3PO4. *Results in Physics* **6**, 651–658.

Lagergren, S. Y. 1898 Zur Theorie der sogenannten Adsorption gelöster Stoffe. *Kungl. Svenska Vetenskapsakademiens Handlingar* **24**, 1–39.

Langmuir, I. 1918 The adsorption of gases on plane surfaces of glass, mica and platinum. *Journal of the American Chemical Society* **40**, 1361–1403.

Lemraski, E. G. & Tahmasebi, Z. 2018 Zero valent iron loaded on SiC nanoparticles as a new adsorbent for removing Pb (lead) and azo dyes from aqueous solution. *Environmental Progress & Sustainable Energy* **37** (5), 1657–1667.

Lohrasbi, S., Kouhbanani, M. A. J., Beheshtkhoo, N., Ghasemi, Y., Amani, A. M. & Taghizadeh, S. 2019 Green synthesis of iron nanoparticles using plantago major leaf extract and their application as a catalyst for the decolorization of azo dye. *BioNanoScience* **9** (2), 317–322.

Luo, F., Yang, D., Chen, Z., Mallavarapu, M. & Naidu, R. 2015 The mechanism for degrading Orange II based on adsorption and reduction by ion-based nanoparticles synthesized by grape leaf extract. *Journal of Hazardous Materials* **296**, 37–45.

Machado, S., Pinto, S. L., Grosso, J. P., Nouws, H. P. A., Albergaria, J. T. & Delerue-Matos, C. 2013 Green production of zero-valent iron nanoparticles using tree leaf extracts. *Science of the Total Environment* **445**, 1–8.

Mu, Y., Jia, F., Ai, Z. & Zhang, L. 2017 Iron oxide shell mediated environmental remediation properties of nano zero-valent iron. *Environmental Science: Nano* **4** (1), 27–45.

Ozkan, Z. Y., Cakirgoz, M., Kaymak, E. S. & Erdim, E. 2018 Rapid decolorization of textile wastewater by green synthesized iron nanoparticles. *Water Science and Technology: A Journal of the International Association on Water Pollution Research* **77** (1–2), 511–517.

Patil, S. S., Shedbalkar, U. U., Truskewycz, A., Chopade, B. A. & Ball, A. S. 2016 Nanoparticles for environmental clean-up: a review of potential risks and emerging solutions. *Environmental Technology & Innovation* **5**, 10–21.

Pattnaik, P., Dangayach, G. S. & Bhardwaj, A. K. 2018 A review on the sustainability of textile industries wastewater with and without treatment methodologies. *Reviews on Environmental Health* **33** (2), 163–203.

Paździor, K., Bilińska, L. & Ledakowicz, S. 2019 A review of the existing and emerging technologies in the combination of AOPs and biological processes in industrial textile wastewater treatment. *Chemical Engineering Journal* **376**, 120597.

Ponder, S. M., Darab, J. G., Bucher, J., Caulder, D., Craig, I., Davis, L., Edelstein, N., Lukens, W., Nitsche, H., Rao, L., Shuh, D. K. & Mallouk, T. E. 2001 Surface chemistry and electrochemistry of supported zerovalent iron nanoparticles in the remediation of aqueous metal contaminants. *Chemistry of Materials* **13** (2), 479–486.

Rahman, N., Abedin, Z. & Hossain, M. A. 2014 Rapid degradation of azo dyes using nano-scale zero valent iron. *American Journal of Environmental Sciences* **10** (2), 157–163.

Raman, C. D. & Kanmani, S. 2016 Textile dye degradation using nano zero valent iron: a review. *Journal of Environmental Management* **177**, 341–355.

Raman, C. D. & Kanmani, S. 2018 Epigallocatechin gallate supported iron particles on dye decolorization and textile wastewater treatment. *Desalination and Water Treatment* **113**, 288–295.

Raman, C. D. & Kanmani, S. 2019 Decolorization of mono azo dye and textile wastewater using nano iron particles. *Environmental Progress & Sustainable Energy* **38** (s1), S366–S376.

Shahwan, T., Sirriah, S. A., Nairat, M., Boyacı, E., Eroğlu, A. E., Scott, T. B. & Hallam, K. R. 2011 Green synthesis of iron nanoparticles and their application as a Fenton-like catalyst for the degradation of aqueous cationic and anionic dyes. *Chemical Engineering Journal* **172** (1), 258–266.

Shih, Y., Tso, C.-P. & Tung, L.-Y. 2010 Rapid degradation of methyl orange with nanoscale zerovalent iron particles. *Journal of Environmental Engineering Management* **20** (3), 137–143.

Sohrabi, M. R., Moghri, M., Fard Masoumi, H. R., Amiri, S. & Moosavi, N. 2016 Optimization of reactive blue 21 removal by nanoscale zero-valent iron using response surface methodology. *Arabian Journal of Chemistry* **9** (4), 518–525.

Sun, Y.-P., Li, X., Cao, J., Zhang, W. & Wang, H. P. 2006 Characterization of zero-valent iron nanoparticles. *Advances in Colloid and Interface Science* **120** (1–3), 47–56.

Ting, A. S. Y. & Chin, J. E. 2020 Biogenic synthesis of iron nanoparticles from apple peel extracts for decolorization of malachite green dye. *Water, Air, & Soil Pollution* **231** (278), 1–10.

Trevizani, J. L. B., Nagalli, A., Passig, F. H., Carvalho, K. Q. d., Schiavon, G. J. & Model, A. N. d. L. 2018 Influence of pH and concentration on the decolorization and degradation of BR red azo dye by ozonization. *Acta Scientiarum Technology* **40**, 1–12.

UNESCO 2018 *The United Nations World Water Development Report 2018: Nature-Based Solutions*. Paris, France.

Ventura-camargo, B. D. C. & Marin-morales, M. A. 2013 Azo dyes: characterization and Toxicity – A review. *Textiles and Light Industrial Science and Technology* **2** (2), 85–103.

Vergili, I., Kaya, Y., Sen, U., Gönder, Z. B. & Aydiner, C. 2012 Techno-economic analysis of textile dye bath wastewater treatment by integrated membrane processes under the zero liquid discharge approach. *Resources, Conservation and Recycling* **58**, 25–35.

Wu, H., Yin, J.-J., Wamer, W. G., Zeng, M. & Lo, Y. M. 2014 Reactive oxygen species-related activities of nano-iron metal and nano-iron oxides. *Journal of Food and Drug Analysis* **22** (1), 86–94.

Yu, L., Qiu, Y., Yu, Y. & Wang, S. 2018 Reductive decolorization of azo dyes via in situ generation of green tea extract-iron chelate. *Environmental Science and Pollution Research International* **25** (18), 17300–17309.

Yuksel, E., Gurbulak, E. & Eyvaz, M. 2012 Decolorization of a reactive dye solution and treatment of a textile wastewater by electrocoagulation and chemical coagulation: techno-economic comparison. *Environmental Progress & Sustainable Energy* **31** (4), 524–535.

First received 5 January 2021; accepted in revised form 27 March 2021. Available online 7 April 2021